A novel influenza A virus mitochondrial protein that induces cell death

Weisan Chen[1], Paul A. Calvo[1], Daniela Malide[1], James Gibbs[1], Ulrich Schubert[1,2], Igor Bacik[1], Sameh Basta[1], Robert O'Neill[3], Jeanne Schickli[3], Peter Palese[3], Peter Henklein[4], Jack R. Bennink[1] & Jonathan W. Yewdell[1]

[1]*Laboratory of Viral Diseases, National Institute of Allergy and Infectious Diseases, Bethesda, Maryland, USA*
[2]*University of Hamburg, Heinrich Pette Institute of Experimental Virology and Immunology, Hamburg, Germany*
[3]*Department of Microbiology, Mount Sinai School of Medicine, New York, NY 10029*
[4]*Institute of Biochemistry, Humboldt University, Berlin, Germany*
W.C. and P.A.C. contributed equally to this study.
Correspondence should be addressed to J.W.Y.; email: jyewdell@nih.gov

While searching for alternative reading-frame peptides encoded by influenza A virus that are recognized by CD8$^+$ T cells, we found an abundant immunogenic peptide encoded by the +1 reading frame of PB1. This peptide derives from a novel conserved 87-residue protein, PB1-F2, which has several unusual features compared with other influenza gene products in addition to its mode of translation. These include its absence from some animal (particularly swine) influenza virus isolates, variable expression in individual infected cells, rapid proteasome-dependent degradation and mitochondrial localization. Exposure of cells to a synthetic version of PB1-F2 induces apoptosis, and influenza viruses with targeted mutations that interfere with PB1-F2 expression induce less extensive apoptosis in human monocytic cells than those with intact PB1-F2. We propose that PB1-F2 functions to kill host immune cells responding to influenza virus infection.

Influenza A virus (IAV) is a major pathogen of humans and animals with the potential to cause catastrophic pandemics, as it has done three times in the 20th century, most lethally in 1918 (ref. 1). IAV possesses eight negative-strand, or antisense, RNA gene segments that are known to encode 10 proteins[2]. In contrast with other negative-strand RNA viruses, a critical portion of the IAV infectious cycle occurs in the nucleus, where viral RNA is produced through the concerted action of three polymerase subunits (PA, PB1 and PB2) and nucleoprotein (NP). At the late stages of infection, M1 and NS2 proteins enter the nucleus, where they induce the shutdown of viral RNA synthesis and promote the export of nucleocapsids (NP and small amounts of polymerase bound to negative-strand RNA) to the cytosol and ultimately to the plasma membrane, where viral budding occurs.

The pathogenicity of IAV is complex, being influenced by each of the eight gene segments. Mutations that substantially affect virus pathogenicity in one host may have no discernible effects on its pathogenicity in other hosts. IAV naturally infects both birds and mammals, and the introduction of genes from avian viruses into human strains is a major factor in creating pandemic strains.

The complete RNA sequence of IAV was reported nearly 20 years ago, and the last defined viral gene product was discovered around that time. We report here the discovery of a novel protein encoded by an open reading frame (ORF) lurking in an alternative reading frame of PB1. The ORF is present in many IAV isolates from a wide range of hosts, including nearly all IAV strains isolated from humans. The new protein has many unusual features compared to other IAV gene products. We show that the protein is not essential for viral replication *in vitro* and provide evidence suggesting that it has a role in modulating the host response to IAV by hastening the death of immune cells.

PB1-F2$_{62–70}$ binds to H-2D^b and is recognized by CD8$^+$ T-lymphocytes

We serendipitously discovered the new gene product in the course of a systematic search for potential antigenic peptides[3] recognized by CD8$^+$ T lymphocytes (T_{CD8+}) that are encoded by non-standard reading frames present in positive-strand RNA of influenza virus A/Puerto Rico/8/34 (H1N1) (PR8) (Mt. Sinai strain). We identified a high-affinity H-2 D^b–binding peptide encoded by the +1 frame of PB1, the gene encoding the PB1 viral polymerase subunit (Fig. 1*a*). This peptide corresponds to residues 62–70 in PB1-F2, a new gene product that we describe below. Immunization of mice with PB1-F2$_{62–70}$ synthetic peptide elicited T_{CD8+} capable of lysing cells exposed to a low concentration of the peptide, similar to the peptide concentration required to obtain lysis of cells exposed to the immunodominant determinant NP$_{366–374}$ by the corresponding T_{CD8+} (Fig. 1*b*). Because the two peptides bind to D^b with similar affinities (Fig. 1*a*), this indicates that PB1-F2$_{62–70}$–specific T_{CD8+} are of similar (high) avidity to that of NP$_{366–374}$-specific T_{CD8+}. Notably, PB1-F2$_{62–70}$–specific T_{CD8+} lysed cells infected with influenza virus (Fig. 1*c*), demonstrating that IAV-infected cells do indeed generate the peptide.

We conclusively showed that the determinant recognized by PB1-F2$_{62–70}$–specific T_{CD8+} originates from PB1-F2 by generating recombinant vaccinia viruses (rVV) that express either wild-type *PB1* or *PB1* with point mutants that selectively disrupt the reading frame of *PB1-F2*. This included mutations introducing a stop codon four residues upstream of the predicted determinant ('PB1-F2*stop*' in Fig. 1*d*) and a substitution of one of the 'dominant anchor residues' of the peptide required for its binding to D^b (Asn$_{65}$→Ser)_ ('PB1-F2*N*→*S*' in Fig. 1*d*). Both mutations completely abrogated recognition of rVV-infected target cells by PB1-F2$_{62–70}$–specific T_{CD8+} (Fig. 1*d*) without decreasing recognition by PB1-specific T_{CD8+} (data not shown). We also generated an rVV expressing the predicted 87-

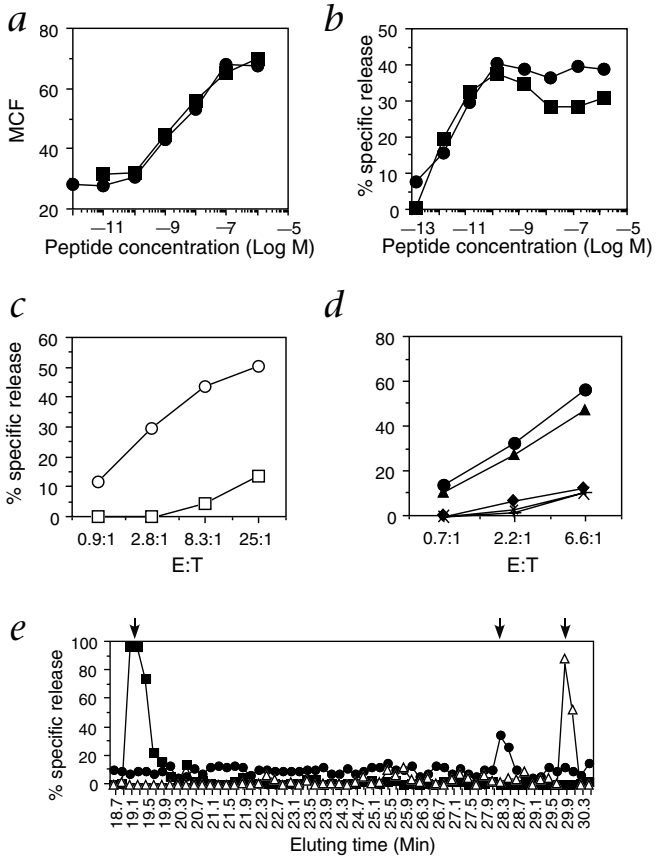

Fig. 1 Characterization of PB1-F2$_{62–70}$ immunogenicity and antigenicity. ***a***, The capacity of peptides to stabilize peptide-receptive D^b molecules at the surface of RMA/S cells was determined by a melting assay as described[25]. The concentration of peptides (in $\log_{10}$ values) (■, NP$_{366–374}$; ● PB1-F2$_{62–70}$)required for protection of half of the D^b molecules (~1 10^{-8} M for each peptide) provides an estimate of their dissociation constant of interaction with D^b. MCF, mean channel fluorescence. ***b***, T$_{CD8+}$ obtained from B6 mice primed with PB1-F2$_{62–70}$ or NP$_{366–374}$ synthetic peptides in incomplete Freund's adjuvant were restimulated *in vitro* with the same peptide and tested for their abilities to lyse cells incubated with corresponding peptides at the indicated concentrations. ■, NP$_{366–374}$; ●, PB1-F2$_{62–70}$. ***c***, PB1-F2$_{62–70}$-specific T$_{CD8+}$ generated as in *b* were tested at the indicated effector-to-target ratios (E:T) for lytic activity against PR8-infected MC57G (H-2^b) cells (○) versus uninfected (□) as determined by ^{51}Cr-release assay. A similar percentage of cells were lysed by NP$_{366–374}$-specific cells in this experiment. ***d***, The lytic activity of PB1-F2$_{62–70}$-specific T$_{CD8+}$ against cells infected with rVVs expressing PB1, the PB1-gene mutants indicated, or control vaccinia virus (VV) was determined by ^{51}Cr-release assay at the E:T indicated. ◆, Cr19 (control VV); ●, PB1-F2; ▲, PB1; +, PB1-F2$_{stop}$; , PB1-F2 *N* → *S*. ***e***, Peptides isolated from PR8-infected EL4 cells and separated by HPLC were used to sensitize ^{51}Cr-labeled RMA/S cells for lysis using T$_{CD8+}$ lines specific for the determinants indicated. Elution positions of synthetic peptides corresponding to the determinants are indicated by arrows at the top of the graph. All synthetic peptide eluted indistinguishably from the naturally processed peptides, as previously shown for NP$_{366–374}$ (ref. 5; ■) and initially shown here for PB1-F2$_{62–70}$ (●) and NS2$_{114–121}$ (△).

residue PB1-F2 polypeptide. This virus induced T$_{CD8+}$ specific for the determinant in B6 mice and, as predicted, was much more efficient than VV-PB1 at generating peptide–MHC class I complexes in antigen-presenting cells *in vitro* (data not shown).

We next HPLC purified PB1-F2$_{62–70}$ from low-M_r acid-soluble material from IAV-infected cells. HPLC fractions were assayed for their abilities to sensitize target cells against T$_{CD8+}$ specific for PB1-F2$_{62–70}$ or, as specificity controls, NP$_{366–374}$ or NS2$_{114–122}$ (a subdominant determinant in the T$_{CD8+}$ response of B6 mice to IAV; ref. 4). Each T$_{CD8+}$ recognized its cognate determinant in fractions that co-eluted with the synthetic version of the peptide (the peak fraction of elution of the synthetic peptide is indicated by the arrows at the top of Fig. 1*e*). This indicates that PB1-F2$_{62–70}$ is a naturally processed peptide generated by PR8-infected cells. Quantification of the amount of peptide recovered by HPLC revealed that infected cells produce considerable amounts of PB1-F2$_{62–70}$: approximately 2,650 molecules per cell. This is comparable to the amounts of NP$_{366–374}$ recovered from the same cells (3,900 molecules per cell) and 10-fold higher than for NS2$_{114–122}$ (271 molecules per cell), as determined by making comparative dilutions of fractions to known amounts of synthetic peptides and taking into account the efficiency of recovery of synthetic peptides added to uninfected cells[5].

PB1-F2$_{62–70}$ is part of a conserved-87-amino-acid ORF

Examination of the sequence of the PR8 genome (Fig. 2) reveals that PB1-F2$_{62–70}$ is part of an 87-residue ORF that is present in 64 of 75 PB1 variants accessible in GenBank, including genes from viruses isolated from numerous mammalian and avian species over the past 70 years (in most other IAV isolates, the ORF is 90 residues). The ORF is not present in PB1 variants from influenza B viruses. The conservation of the PB1-F2 ORF in IAV cannot be attributed to severe constraints on the corresponding in-frame sequence of PB1, as stop codons are introduced into the PB1-*F2* reading frame in a number of viruses, particularly isolates from swine (of the 11 viruses with PB1-*F2* interrupted, 6 were isolated from swine). In addition, once a single stop codon is introduced among swine isolates, additional stop codons accumulate in subsequent isolates.

Notably, PB1 is the only gene in PR8 that does not possess an A or G nucleotide in the –3 position relative to the start codon, making it likely that initiation of PB1 translation is relatively inefficient, according to Kozak's analysis[6]. The next two potential start codons are also suboptimal, whereas the predicted start codon of PB1-*F2* has G in both the –3 and +4 positions. These features suggest that PB1-F2 translation is initiated by ribosomal scanning as opposed to internal ribosomal entry or other mechanisms. Ribosomal scanning is known to occur in other RNA viruses, including influenza B virus[7], as a means to generate multiple products from a single gene.

```
AGCGAAAGCAGGCAAACCATTTGAATGGATGTCAATCCGACCTTACTTTTCTTAAAAGTGC- 60
CAGCACAAAATGCTATAAGCACAACTTTCCCTTATACCGGAGACCCTCCTTACAGCCATG - 120
                                                          M
GGACAGGAACAGGATACACCATGGATACTGTCAACAGGACACATCAGTACTCAGAAAAGG - 180
 G  Q  E  Q  D  T  P  W  I  L  S  T  G  H  I  S  T  Q  K  R
CAAGATGGACAACAAACACCGAAACTGGAGCACCGCAACTCAACCCGATTGATGGGCCAC - 240
 Q  D  G  Q  Q  T  P  K  L  E  H  R  N  S  T  R  L  M  G  H
TGCCAGAAGACAATGAACCAAGTGGTTATGCCCAAACAGATTGTGTATTGGAAGCAATGG - 300
 C  Q  K  T  M  N  Q  V  V  M  P  K  Q  I  V  Y  W  K  Q  W
CTTTCCTTGAGGAATCCCATCCTGGTATTTTTGAAAACTCGTGTATTGAAACGATGGAGG - 360
 L  S  L  R  N  P  I  L  V  F  L  K  T  R  V  L  K  R  W  R
TTGTTCAGCAAACACGAGTAG                                      382
 L  F  S  K  H  E  *
```

Fig. 2 DNA and amino acid sequence of novel ORF in the PB1 gene. Shown is the 3′ sequence of the *PB1* positive strand, with the predicted nucleotide sequence for the alternative ORF (in the +1 reading frame relative to PB1) in bold and the predicted amino acid sequence. Upstream ATG triplets are in bold with yellow highlight; the established ATG for *PB1* is also underlined. The predicted ATG of the new ORF is in red with a red underline. PB1-F2$_{62–70}$ is indicated by blue italics and underline.

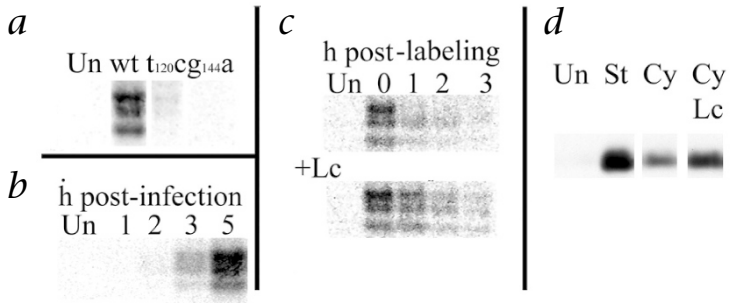

Fig. 3 Biochemical characterization of PB1-F2. ***a***, MDBK cells were infected for 5 h with WSN^{7+1} or mutant viruses, radiolabeled with [^{35}S]Met and the material in detergent extracts reactive with antibodies against PB1-F2 was analyzed by SDS–PAGE. ***b***, MDBK cells were infected with WSN^{7+1} for the times indicated, then radiolabeled and detergent extracts analyzed as described in (*a*). ***c***, MDBK cells were infected with WSN^{7+1} for 4 h and radiolabeled with [^{35}S]Met for 5 min and chased for 0, 1, 2, and 3 h with unlabeled Met; detergent extracts were analyzed as described in (*a*). Bottom of panel shows samples from cells incubated with 50 M lactacystin (Lc) during Met starvation and radiolabeling and then with 10 M lactacystin during the chase period. ***d***, MDBK cells were infected for 5 h with WSN^{7+1} and either immediately harvested for western blotting using antibodies against PB1-F2 ('St' for start) or incubated for 2 h with medium supplemented with 25 g ml^{-1} cycloheximide (Cy) in the absence or presence of 25 g ml^{-1} lactacystin (Lc) and then collected for western blotting. Uninfected (Un) cells are in the first lane.

PB1-F2 has multiple molecular species and a short half-life

To determine whether PB1-F2 is a *bona fide* IAV gene product, we affinity-purified rabbit antibodies elicited by a synthetic peptide corresponding to the predicted N terminus. We used antibodies against PB1-F2 to collect [^{35}S]Met proteins from detergent lysates of MDBK cells infected at the same MOI with one of three recombinant WSN influenza viruses generated using reverse genetics[8] to encode a PR8 PB1. One virus (WSN^{7+1}) expresses the wild-type gene, the others express this gene with either (i) a T → C substitution at nucleotide 120 in PB1, introducing an alteration in the proposed Met start codon to Ser without affecting the standard reading frame, or (ii) a G → A substitution at nucleotide 144, introducing a stop codon after translation of only eight residues of PB1-F2, and a Met → Ile substitution in PB1 at position 40. This is a natural substitution in the avian influenza virus A/Chicken/HK/739/94, an isolate with an interrupted PB1-F2.

Antibodies against PB1-F2 recognized three protein species migrating close to the predicted M_r of PB1-F2 (10.5 kD) (Fig. 3*a*). These species were not present in lysates from uninfected cells. Introduction of the stop codon resulted in complete loss of the three species, whereas modification of the initiating Met → Ser resulted in a 12-fold decrease in the amount of protein recovered. Initiation at Ser has been reported for a number of viral and cellular proteins[6,9] and is consistent with the idea that the structure of the PB1 RNA strongly favors translation at the predicted PB1-F2 start codon.

We next determined the kinetics of PB1-F2 expression by pulse radiolabeling cells at various times after infection with WSN^{7+1}. We first detected PB1-F2 expression two hours post infection (p.i.), with maximal translation occurring three hours later (after which cells begin to die) (Fig. 3*b*). A pulse–chase experiment showed that PB1-F2 recovered from detergent lysates exhibits a half-life of approximately 30 min (Fig. 3*c*) and that this could be prolonged by treating cells with lactacystin (Lc) (Fig. 3*c*, bottom panel), a highly specific inhibitor of proteasomes[10]. We confirmed that this represented true proteasome-dependent degradation of PB1-F2 (as opposed to decreased detergent solubility, for example) by western blotting whole-cell lysates solubilized by boiling cells in SDS-PAGE sample buffer[11]. Cells were infected with $WSN^{7+1}$for five hours (Fig. 4*d*) and treated for two hours with the protein-synthesis inhibitor cycloheximide (Cy) alone or with lactacystin (Lc). Unlike the metabolic labeling, western blotting detected only a single species of PB1-F2 (which comigrates with a synthetic peptide corresponding to full-length PB1-F2; data not shown). This may be related to the observation that the middle of the three radiolabeled species recovered exhibits the greatest stability in the absence of proteasome inhibitors (Fig. 3*c*). The instability of PB1-F2 could help explain why $PB1\text{-}F2_{62\text{–}70}$ is recovered in similar amounts to $NP_{366\text{–}374}$, despite the relatively low rate of translation of the protein relative to NP (< 10%).

PB1-F2 localizes to the mitochondria and induces cell death

We next examined the subcellular localization of PB1-F2 by indirect immunofluorescence of PR8-infected MDBK cells using confocal microscopy. PB1-F2–specific staining was detected in 137 of 357 cells (38%) counted in 10 randomly chosen fields (a representative field is shown in Fig. 4*a*). Flow cytometry of permeabilized cells con-

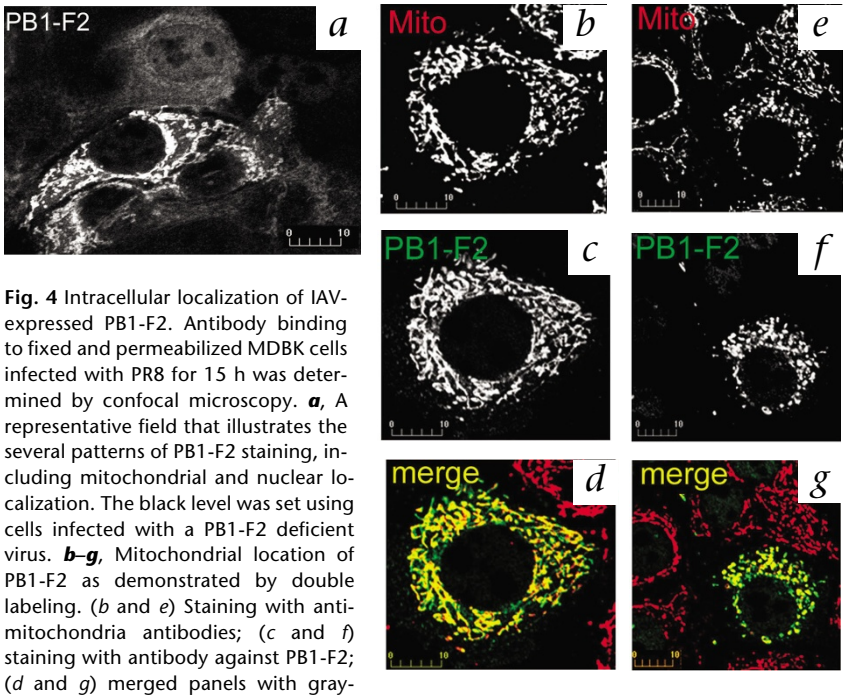

Fig. 4 Intracellular localization of IAV-expressed PB1-F2. Antibody binding to fixed and permeabilized MDBK cells infected with PR8 for 15 h was determined by confocal microscopy. ***a***, A representative field that illustrates the several patterns of PB1-F2 staining, including mitochondrial and nuclear localization. The black level was set using cells infected with a PB1-F2 deficient virus. ***b–g***, Mitochondrial location of PB1-F2 as demonstrated by double labeling. (*b* and *e*) Staining with anti-mitochondria antibodies; (*c* and *f*) staining with antibody against PB1-F2; (*d* and *g*) merged panels with gray-scale images assigned colors. Scale bars are in micrometers. Mitochondria in the PB1-F2–expressing cell in the left panels exhibit typical morphology (parts of two other PB1-F2 negative cells are also seen at one and five o'clock in the panels); those in the PB1-F2–expressing cell in the right panels are fragmented (parts of six PB1-F2-negative cells are also seen in the panels). All cells in both fields express abundant amounts of NP (data not shown).

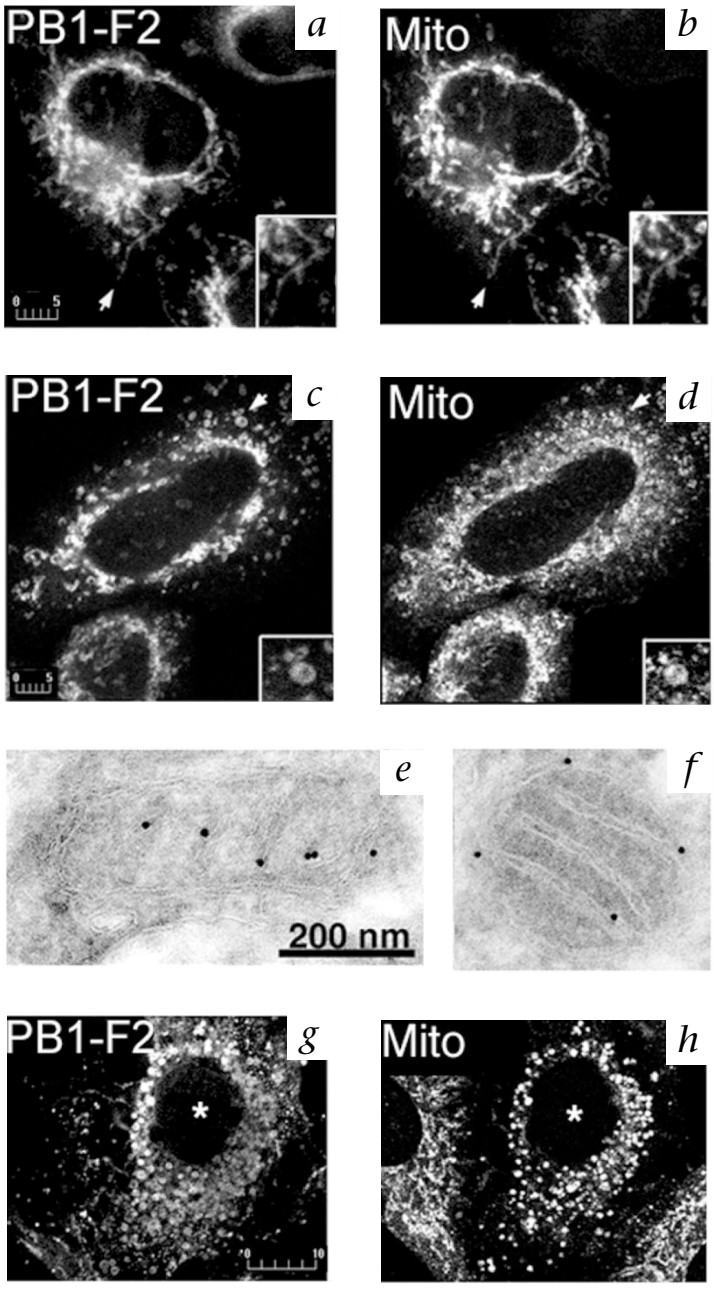

Fig. 5 Intracellular localization of transfected and microinjected PB1-F2. ***a–d***, HeLa cells transfected for 15 h with cDNA encoding PB1-F2 were fixed and stained as in Fig. 4 using antibodies against PB1-F2 (*a* and *c*) and against mitochondria (*a* and *d*); insets represent higher magnification of region indicated by arrowheads. Cell with normal-looking (*a* and *b*) and morphologically altered (*c* and *d*) mitochondria are shown. Insets, high magnification of areas identified by arrows, with typical tubular mitochondria (*a* and *b*) or rounded mitochondria (*c* and *d*). Parts of neighboring cells (two in left panels and one in right panels) are also visible. ***e–f***, Transfected HeLa were processed for Immunogold labeling with antibodies against PB1-F2, which localize to inner and outer mitochondrial membranes. Scale bar, 200 nm. ***g–h***, MDBK cells plated on gridded coverslips were microinjected with 50 M PB1-$F2_{syn}$ solution . Cells were allowed to recover for 4 h, fixed and processed for immunocytochemistry as in Fig. 4 using antibodies against mitochondria and against PB1-F2. Grid coordinates were used to locate a microinjected cell (*), which displays rounded mitochondria. Normal, tubular mitochondria are visible in the parts of two neighboring non-injected cells that can be seen. Scale bars are in micrometers (*a–d*, *g* and *h*) and in nanometers (*e–f*).

firmed that 45% of infected cells specifically bound antibodies against PB1-F2 (data not shown). Treating cells with a proteasome inhibitor for the last 2 hours of infection increased the fraction of PB1-F2–positive cells detected by confocal microscopy to approximately 50% of the infected cells (279 positives out or 548 cells counted in 10 randomly chosen fields). This provides a minimal estimate of the fraction of infected cells that express PB1-F2. A similar percentage of cells were lysed by T_{CD8+} specific for NP as were lysed by T_{CD8+} specific for PB1-F2 (data not shown), indicating that PB1-F2 is expressed in all infected cells in amounts sufficient to generate the requisite number of peptide–class I complexes for T_{CD8+} recognition.

In approximately 55% of PB1-F2–positive cells, staining localized largely to mitochondria, as identified by the colocalization of staining produced by autoimmune human antiserum specific to mitochondria (Fig. 4*b–g*) or Mitotracker Red dye (data not shown). In the other 45% of PB1-F2–positive cells, PB1-F2 was present in the nucleus or in the nucleus and cytoplasm (Fig. 4*a*). The amount of PB1-F2 detected differed considerably between cell types, with the strongest staining occurring in the mitochondria. PB1-F2 was present in mitochondria of some cells as soon as the protein could be detected after infection (as early as 90 min p.i.), showing that mitochondrial localization does not require prolonged expression. Notably, some cells expressing mitochondrial PB1-F2 exhibited alteration of the normal tubular mitochondrial morphology (Fig. 4*b*) to a more rounded, vesicular form (Fig. 4*e*). This was associated with a loss of mitochondrial membrane potential, as indicated by decreased staining with Mitotracker Red (data not shown). These alterations in mitochondria, which are frequently associated with the induction of cell death, were also seen in PR8-infected cells that fail to express detectable PB1-F2, but at a lower frequency.

Additional findings indicate that the localization of PB1-F2 to the mitochondria is intrinsic to the protein, whereas nuclear/cytoplasmic localization requires expression in the context of IAV infection. Expression of PB1-F2 by infection with rVV-PB1-F2 (data not shown) or by transfection of HeLa cells with a cDNA under the control of the cytomegalovirus resulted in strong mitochondrial accumulation and little or no detectable staining of the nucleus or nuclear membrane (Fig. 5). In some PB1-F2–expressing cells, mitochondria exhibited the tubular pattern typical in normal non-transfected cells (Fig. 5*a* and *b*). In other cells, mitochondria exhibited rounding and occasionally a swollen pattern consistent with fragmentation (Fig. 5*c* and *d*). Alterations in mitochondrial morphology were associated with the perturbation of mitochondrial membrane potential, as indicated by decreased staining with the potential-sensitive dye Mitotracker Red (data not shown). Immunogold electron microscopy confirmed that PB1-F2 was nearly exclusively located in the mitochondria of transfected cells, and also revealed that the protein is associated with both outer and inner mitochondrial membranes in morphologically normal mitochondria (Fig. 5*e* and *f*).

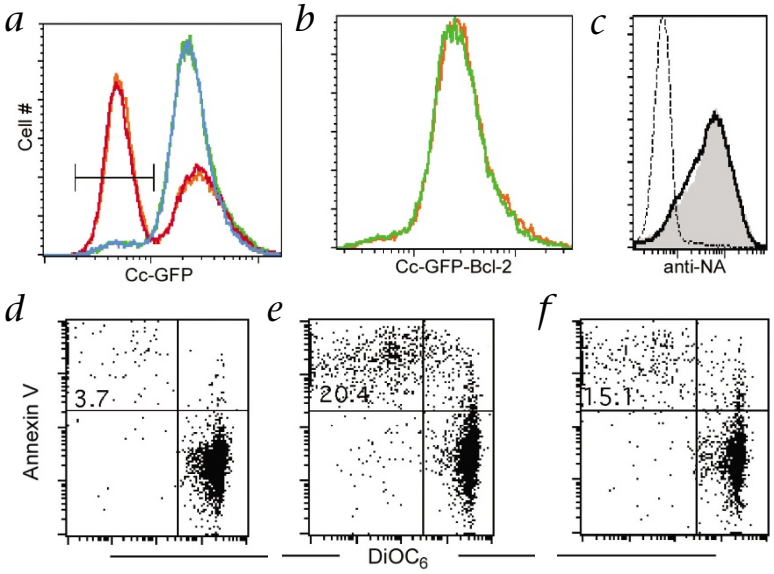

Fig. 6 PB1-F2 mediated induction of apoptosis. ***a*** and ***b***, HeLa cells expressing Cc-GFP without (*a*) or with Bcl-2 (*b*) were incubated without or with 300 nM PB1-F2$_{syn}$ and the amount of mitochondrial-associated GFP in permeabilized cells was assessed by flow cytometry as described[12]. Apoptosis is associated with a loss of Cc-GFP from mitochondria and a leftward shift in the histogram. To show that cytotoxicity of cells not transfected with Bcl-2 gene is due to the peptide itself and not a contaminant, PB1-F2$_{syn}$ was treated with agarose beads conjugated to a protease mixture (pepsin, papain, trypsin-TPCK) or to avidin (as control). Green, no peptide; orange, PB1-F2$_{syn}$; blue, PB1-F2$_{syn}$ incubated with protease beads; red, PB1-F2$_{syn}$ incubated with avidin beads. Percentages of Cc negative cells (in bracket indicated in *a*): no peptide, 7%; PB1-F2$_{syn}$, 55%; protease-treated PB1-F2$_{syn}$, 7%; avidin-treated PB1-F2$_{syn}$, 53%. ***c–f***, U937 cells were infected with PR8 or PB1-F2–deficient PR8 at a MOI of 2 PFU per cell for 12 h. *c*, NA expression was determined by flow cytometry using the NA-specific mAb NA2-1C1; uninfected cells, dotted line histogram; wild-type virus, gray-filled histogram; mutant, solid-line histogram. Cells were incubated with 50 nM DiOC$_6$ and annexin V–phycoerythrin and analyzed by flow cytometry. *d*, Uninfected; *e*, wild-type infected; and *f*, PB1-F2–deficient infected cells. The percentage of annexin V^{Hi} DiOC$_{6Low}$ cells is shown in the upper left quadrant of the dot plot.

The effect of PB1-F2 on mitochondrion structure and function was confirmed by microinjection of MDBK cells with a synthetic peptide corresponding to the full-length protein (PB1-F2$_{syn}$). PB1-F2$_{syn}$ localized strongly to mitochondria (and weakly to the endoplasmic reticulum), resulting in rounding and possible fragmentation of mitochondria, nuclear shrinkage (Fig. 5*g* and *h*) and ultimately cell death. By contrast, injection of control peptides of similar length synthesized and purified by the same methodology had no effect on mitochondrial structure or cell viability (data not shown). In the course of the microinjection experiments, we noticed that local application of PB1-F2$_{syn}$ to cells induced cell death. Indeed, exposure of MDBK cells for 4 hours to medium containing as little as 50 nM PB1-F2$_{syn}$ induced cell death (data not shown).

To further explore the mechanism of PB1-F2$_{syn}$ cytotoxicity, we used HeLa cells expressing cytochrome *c* tagged with green fluorescent protein (Cc-GFP-HeLa). Release of cytochrome *c* from mitochondria, which can be quantified by flow cytometry of digitonin permeabilized cells, accompanies the induction of apoptosis in these cells[12], and Cc-GFP release is not induced by necrosis (J. Goldstein & D.R. Green, pers. comm.). Incubation of Cc-GFP-HeLa cells with 300 nM PB1-F2$_{syn}$ induced the release of Cc-GFP from mitochondria in 55% of cells, compared to a background value of 7% in untreated cells (Fig. 6*a*). Apoptosis is induced by the PB1-F2$_{syn}$ itself and not by any contaminants in the peptide preparation, because (i) apoptosis was eradicated by incubating the preparation with beads coupled to proteases but not control beads coupled to avidin (Fig. 6*a*) and (ii) several other peptides of similar length synthesized in the same manner were not cytotoxic (data not shown). In addition, under identical conditions PB1-F2$_{syn}$ did not induce the release of Cc-GFP from Cc-GFP-HeLa cells co-transfected with Bcl-2, which increases cellular resistance to apoptosis[12] (Fig. 6*b*).

Influenza virus is reported to induce apoptosis in human monocytes[13], a process that involves at least one defined IAV gene product, NS1 (ref. 14). We examined the participation of PB1-F2 in this process by infecting the human monocyte cell line U937 with control PR8 (Fig. 6*e*) or PR8 with the *PB1* variant containing the G → A substitution at position 144 (Fig. 6*f*). At 12 hours after infection, apoptosis was measured by increased binding of annexin V (a measure of translocation of phosphatidylserine to the outer leaflet of plasma membrane) and by the decreased capacity of mitochondria to accumulate the membrane potential-sensitive dye DiOC$_6$ (3,3′-dihexyloxacarbocyanine iodide). Expression of PB1-F2 was associated with an approximately 50% increase in the number of annexin^{Hi} DiOC$_{6Low}$ cells (upper left quadrant in the dot plots) relative to uninfected cells (Fig. 6*d*). Annexin^{Hi} cells were apoptotic and not necrotic, as they excluded the nuclear dye ethidium homodimer (data not shown). Cells infected with wild-type and mutant virus expressed nearly identical amounts of viral neuraminidase glycoprotein, as detected by the binding of a NA-specific mAb (compare dark line to gray solid histogram, Fig. 6*c*). Thus, the mutant phenotype cannot be explained by diminished viral gene expression. In addition, the loss of PB1-F2 expression was associated with a decrease in apoptosis in freshly isolated human monocytes as determined by annexin V binding and propidium iodide exclusion. This effect was seen in monocytes obtained from three of four donors, with an average decreased apoptosis of 56% associated with the absence of PB1-F2 (averages from three experiments: 17.7% annexin^{Hi} (wild-type) versus 11.3% annexin^{Hi} (mutant)). In contrast, we did not see substantial effects of PB1-F2 expression on virus-induced apoptosis in the epithelial cell lines MDCK, MDBK, A549 and HeLa, the first three of which support productive influenza virus infection.

Discussion

PB1-F2 joins other viral proteins known to induce apoptosis, including Vpr of human immunodeficiency virus (HIV), which like PB1-F2 is a small protein that localizes to mitochondria and the nucleus[15]. According to the NNPREDICT algorithm, PB1-F2 has a propensity to form an amphipathic helix extending from Leu$_{69}$ to Phe$_{83}$ (ref. 16). Within the predicted helix, five basic residues occur from Lys$_{73}$ to Arg$_{81}$. This resembles the Arg-rich domains of Vpr and HIV Tat that are required for membrane translocation. We are presently investigating whether, like Vpr, PB1-F2 forms membrane pores.

Viral gene products evolve to foster transmission between hosts: how might PB1-F2 contribute to the evolutionary fitness of IAV?

The PB1-F2–deficient viruses we produced exhibited no obvious differences in their ability to grow in eggs, MDBK or MDCK cells, so PB1-F2 is clearly dispensable for replication in at least some host cells. On the other hand, PB1-F2 expression accelerated IAV-induced apoptosis in a cell type–specific manner: a monocytic cell line and freshly isolated human monocytes were affected, whereas the epithelial cell lines we tested were spared. This indicates that PB1-F2 may function *in vivo* to disable IAV-infected monocytes or other host innate immune cells (such as the subset of NK cells specific for viruses that express sialic acid glycoproteins[17]) that impede viral transmission. In this scenario, PB1-F2 acts in *cis*: it accelerates apoptosis in cells that synthesize it. In addition, the cytotoxicity of PB1-$F2_{syn}$ suggests that PB1-F2 may also act in *trans*: extracellular PB1-F2 released by infected cells could potentially inactivate host cells recruited to the site of infection.

A possible clue to the involvement of PB1-F2 in IAV pathogenicity in humans is the finding that during the introduction into humans of the highly pathogenic H2N2 and H3N2 pandemic viruses, PB1 was the sole non-glycoprotein gene segment derived from avian viruses[18]. It will be of interest to examine the role of PB1-F2 in highly lethal avian influenza virus infections associated with massive loss of immune cells[19], and to determine the status of the PB1-F2 reading frame in IAV sequences amplified from tissues of victims of the 1918 IAV pandemic[20] to assess whether it may have contributed to the lethality of this virus.

Methods

Cells and viruses. MDCK and MDBK cells (obtained from ATCC) and transfected HeLa cells (obtained from D. Green) were maintained in DMEM supplemented with 10% FBS. EL4 and MC57/G cells were maintained in RPMI-1640 containing 10% FBS, 5 10^{-5} M 2-mercaptoethanol and 2 mM Glutamax (Life Technologies, Gaithersburg, Maryland). IAVs were propagated in 10-day-old embryonated hen's eggs (Truslow Farms, Chestertown, Maryland) for 2 d at 35 °C, and used as infectious allantoic fluid. Recombinant vaccinia and influenza viruses were generated as described[21,22]. The sequences of modified genes were confirmed by sequencing of viral genomes. Recombinant influenza viruses generated in MDCK cells were adapted to growth in eggs by three serial passages in eggs. Influenza viruses were titered by plaque assay in MDCK cells.

Immunofluorescence and immuno-EM localization of PB1-F2. IAV infected-MDBK cells grown on 0.17-mm glass coverslips were fixed for 20 min with 3% (w/v) paraformaldehyde in PBS and permeabilized for 2 min with 0.1% (v/v) Nonidet P-40. All solutions used subsequently contained 0.1% Brij 58 (Pierce, Rockford, Illinois) and 5% (v/v) donkey serum. Fixed cells were incubated overnight with antibodies specific for PB1-F2, with human autoimmune serum specific for mitochondria (Immunovision, Springdale, Arizona) and with H16-L10, an antibody specific for NP (data not shown). Antibodies were detected using fluorochrome-conjugated secondary antibodies prepared from donkeys (Jackson Immunoresearch, West Grove, Pennsylvania). Images were acquired by simultaneous scanning using a Bio-Rad (Hercules, California) 1024 laser-scanning confocal microscope. For Immunogold labeling, HeLa cells transfected with PB1-F2 for 15 h were fixed with a mixture of 2% paraformaldehyde and 0.2% glutaraldehyde. Ultrastructural immunocytochemistry on frozen ultrathin sections was done as described using antibodies against PB1-F2 and (as secondary antibodies) gold-conjugated antibodies against rabbit[23].

Immunoprecipitation. MDBK cells (1 10^7) were infected in a 10-cm tissue-culture dish with WSN^{7+1} virus at a multiplicity of infection (MOI) of 0.1 plaque forming units (PFU) per cell. At the appropriate time, cells were trypsinized, washed once with PBS and incubated for 30 min at 37 °C in Met-free DMEM and then for 5 min at 37 °C in the same medium containing 2 mCi ml^{-1} [^{35}S]Met. Ice-cold complete medium was added to the cells and cells were centrifuged at 13,000*g* for 2 min at 4 °C. The medium was aspirated and the cell pellets were snap-frozen on dry ice. Cell pellets were lysed for 10 min on ice in 2% deoxycholate (DOC) in CHAPS buffer (100 mM NaCl, 50 mM Tris-Cl, pH 8.0, 5 mM EDTA, 0.5% CHAPS) containing a protease inhibitor cocktail (Complete; Roche). Lysates were clarified by centrifugation for 15 min at 13,000*g* at 4 °C. Triton wash buffer (50 mM Tris-Cl, pH 7.4, 300 mM NaCl, 0.1% Triton X-100) was added and lysates were precleared by 1 h incubation at 4 °C with protein A–conjugated beads (Amersham Pharmacia Biotech, Piscataway, New Jersey) coupled with normal rabbit serum on a rotator. Lysates were then incubated for 2 h at 4 °C with protein A–beads coupled to antibodies specific for PB1-F2. Antibodies specific for PB1-F2 were prepared from serum obtained from rabbits hyperimmunized with Titermax adjuvant (Sigma) containing synthetic peptide corresponding to the 15 residues at the predicted N terminus of PB1-F2 with a COOH-terminal Cys added to enable disulfide coupling to keyhole limpet hemocyanin (MGQE-QDTPWILSTGHC). Specific antibodies were purified against the immunizing peptide coupled to Sulfolink (Pierce) according to the manufacturer's instructions. The beads were washed twice with Triton wash buffer and once with SDS-DOC wash buffer (50 mM Tris-Cl, pH 7.4, 300 mM NaCl, 0.1% SDS, 0.1% DOC) and the purified proteins were analyzed by SDS–PAGE. Radioactivity was visualized and digitally reproduced using a PhosphorImager (Molecular Dynamics, Sunnyvale, California).

Peptide isolation. Peptides were isolated from 1 10^9 PR8-infected EL4 cells and separated by HPLC as described[24]. One-tenth of each HPLC fraction was used to sensitize ^{51}Cr-labeled RMA/S cells that were incubated overnight at 26 °C to maximize the numbers of peptide-receptive class I molecules.

Peptide synthesis. Solid-phase peptide synthesis was done using a Perkin-Elmer MilliGen 9050 automated peptide synthesizer using Fmoc strategy. PB1-$F2_{syn}$ was purified to homogeneity by reverse-phase HPLC. The product was > 99% pure as determined by analytical HPLC and positive-ion electrospray ionization mass spectroscopy. Details of PB1-$F2_{syn}$ synthesis and purification and further characterization of the peptide will be published elsewhere (P. Henklein *et al.*, manuscript in preparation).

Western-blot analysis. MDBK cells were infected in suspension with PR8 at MOI of 2 PFU per cell, incubated at 37 °C on a rotator for the indicated time and then washed and lysed by addition of Laemmli sample buffer heated to 95 °C. Lysed cells (1 10^6 cell equivalents per lane) were loaded on a Tris/Tricine polyacrylamide gel (16%). Gels were electrophoresed at constant amperage until the bromophenol blue dye reached the bottom of the gel. Proteins were electrically transferred to Immobilon-P membrane (Millipore, Bedford, Massachusetts), which was then blocked at 4 °C overnight with 0.4% Tween-20, 5% bovine serum albumin in PBS (TBS). Membranes were incubated with antibody against PB1-F2 at 1 g ml^{-1} in TBS with 5% sheep serum for 1 h at 4 °C, then washed and incubated with horseradish peroxidase conjugated to sheep antibody against rabbit immunoglobulin (Roche) at a dilution of 1:1,000 in TBS with 5% sheep serum. Membranes were then incubated with Supersignal enhanced chemoluminescence substrate (Pierce) and immediately exposed to BioMax MR1 film (Kodak, Rochester, New York). Images were digitally generated from scanned films.

Acknowledgments

We thank B. Buschling for technical assistance; A. Weisberg for cryo-electron microscopy; K. Bruns for secondary structure predictions using NNPREDICT; D. Green for generously and expeditiously providing cytochrome c–transfected cells and unpublished data; and D. Tscharke for critical comments on the manuscript and assistance with the graphics.

RECEIVED 22 AUGUST; ACCEPTED 30 OCTOBER 2001

1. Webster, R.G. Influenza virus: transmission between species and relevance to emergence of the next human pandemic. *Arch. Virol. Suppl.* **13**, 105–113 (1997).
2. Lamb, R.A. The influenza virus RNA segments and their encoded proteins. in *Genetics of Influenza Viruses* (eds. Palese, P. & Kingsbury, D. W.) 26–69 (Springer, New York, 1983).
3. Mayrand, S.M. & Green, W.R. Non-traditionally derived CTL epitopes: exceptions that prove the rules? *Immunol. Today* **19**, 551–556 (1998).
4. Vitiello, A. *et al.* Immunodominance analysis of CTL responses to influenza PR8 virus

reveals two new dominant and subdominant Kb-restricted epitopes. *J. Immunol.* **157**, 5555–5562 (1996).
5. Rötzschke, O. *et al.* Isolation and analysis of naturally processed viral peptides as recognized by cytotoxic T cells. *Nature* **348**, 252–254 (1990).
6. Kozak, M. Structural features in eukaryotic mRNAs that modulate the initiation of translation. *J. Biol. Chem.* **266**, 19867–19870 (1991).
7. Williams, M.A. & Lamb, R.A. Effect of mutations and deletions in a bicistronic mRNA on the synthesis of influenza B virus NB and NA glycoproteins. *J. Virol.* **63**, 28–35 (1989).
8. Pleschka, S. *et al.* A plasmid-based reverse genetics system for influenza A virus. *J. Virol.* **70**, 4188–4192 (1996).
9. Becerra, S.P., Koczot, F., Fabisch, P. & Rose, J.A. Synthesis of adeno-associated virus structural proteins requires both alternative mRNA splicing and alternative initiations from a single transcript. *J. Virol.* **62**, 2745–2754 (1988).
10. Fenteany, G. *et al.* Inhibition of proteasome activities and subunit-specific amino-terminal threonine modification by lactacystin. *Science* **268**, 726–731 (1995).
11. Laemmli, U.K. Cleavage of structural proteins during the assembly of the head of bacteriophage T4. *Nature* **227**, 680–685 (1970).
12. Waterhouse, N.J. *et al.* Cytochrome *c* maintains mitochondrial transmembrane potential and ATP generation after outer mitochondrial membrane permeabilization during the apoptotic process. *J. Cell Biol.* **153**, 319–328 (2001).
13. Schultz-Cherry, S., Krug, R.M. & Hinshaw, V.S. Induction of apoptosis by influenza virus. *Semin. Virol.* **8**, 491–495 (1998).
14. Schultz-Cherry, S., Dybdahl-Sissoko, N., Neumann, G., Kawaoka, Y. & Hinshaw, V.S. Influenza virus ns1 protein induces apoptosis in cultured cells. *J. Virol.* **75**, 7875–7881 (2001).
15. Ferri, K.F., Jacotot, E., Blanco, J., Este, J.A. & Kroemer, G. Mitochondrial control of cell death induced by HIV-1–encoded proteins. *Ann. N.Y. Acad. Sci.* **926**, 149–164 (2000).
16. Kneller, D.G., Cohen, F.E. & Langridge, R. Improvements in protein secondary structure prediction by an enhanced neural network. *J. Mol. Biol.* **214**, 171–182 (1990).
17. Mandelboim, O. *et al.* Recognition of haemagglutinins on virus-infected cells by NKp46 activates lysis by human NK cells. *Nature* **409**, 1055–1060 (2001).
18. Kawaoka, Y., Krauss, S. & Webster, R.G. Avian-to-human transmission of the PB1 gene of influenza A viruses in the 1957 and 1968 pandemics. *J. Virol.* **63**, 4603–4608 (1989).
19. Van Campen, H., Easterday, B.C. & Hinshaw, V.S. Destruction of lymphocytes by a virulent avian influenza A virus. *J. Gen. Virol.* **70 (Pt 2)**, 467–472 (1989).
20. Taubenberger, J.K., Reid, A.H. & Fanning, T.G. The 1918 influenza virus: a killer comes into view. *Virology* **274**, 241–245 (2000).
21. Chakrabarti, S., Brechling, K., & Moss, B. Vaccinia virus expression vector: coexpression of β-galactosidase provides visual screening of recombinant virus plaques. *Mol. Cell Biol.* **5**, 3403–3409 (1985).
22. Garcia-Sastre, A. *et al.* Influenza A virus lacking the NS1 gene replicates in interferon-deficient systems. *Virology* **252**, 324–330 (1998).
23. Liou, W., Geuze, H.J. & Slot, J.W. Improving structural integrity of cryosections for immunogold labeling. *Histochem. Cell Biol.* **106**, 41–58 (1996).
24. Chen, W., Anton, L.C., Bennink, J.R. & Yewdell, J.W. Dissecting the multifactorial causes of immunodominance in class I–restricted T cell responses to viruses. *Immunity.* **12**, 83–93 (2000).
25. Chen, W., Yewdell, J.W., Levine, R.L. & Bennink, J.R. Modification of cysteine residues in vitro and in vivo affects the immunogenicity and antigenicity of major histocompatibility complex class I–restricted viral determinants. *J. Exp. Med.* **189**, 1757–1764 (1999).